Digest Journal of Nanomaterials and Biostructures Vol. 17, No. 4, October-December 2022, p. 1125-1134

Study on the photodynamic performance of non-stoichiometric nano-tungsten oxide probe

L. R. Dai, J. Zhou, X. F. Gao, J. B. Li, B. Y. Feng, Y. Z. Yao, Y. M. Wang, W. W. Cui, X. J. Li*

School of Materials Science and Chemical Engineering, Harbin University of Science and Technology, Harbin, China

Photodynamic therapy (PDT) is an effective and new method for tumor therapy but limited by the poor penetration depth of tissue of ultraviolet or visible light as irradiation source. Herein a near-infrared light-responsive $W_{18}O_{49}$ nanoprobe was synthesized by the solvothermal method for PDT. The structure, morphology, infrared absorption property and the photodynamic performance were analyzed. The results showed that the samples had high crystallinity, uniform and dispersed spindle morphology and an obvious absorption of NIR light. Under the irradiation of 808 nm near-infrared light, 1,3-diphenylisobenzofuran (DPBF) was used as a capture agent for singlet oxygen, and the samples showed excellent photodynamic performance. Then *in vitro* cell experiments further indicated that the samples good biocompatibility and an evident inhibition effect on tumor cell growth under near-infrared irradiation. The nanoprobe will have a wide application prospect in photodynamic cancer therapy.

(Received May 4, 2022; Accepted October 6, 2022)

Keywords: Tungsten oxide, Solvothermal method, Near infrared light, Photodynamic, Singlet oxygen

1. Introduction

In recent years, cancer has become one of the diseases with the highest mortality rate. Traditional cancer treatment methods such as surgery, radiotherapy and chemotherapy often have great side effects. There are many limitations in the treatment process, such as easy recurrence, low cure rate, and destruction of the immune system [1-3]. There is an urgent need to develop a therapeutic approach with low side effects for future clinical cancer treatment [4,5]. Photodynamic Therapy (PDT) is an emerging and effective tumor treatment method, which has the advantages of low aggressiveness, little harm to human body and good curative effect. This treatment method has achieved many therapeutic results in clinical application [6,7]. The mechanism of PDT is that

* Corresponding author: lixuejiao@hrbust.edu.cn

https://doi.org/10.15251/DJNB.2022.174.1125

photosensitizer molecules will selectively enrich and enter tumor cells. And the cell apoptosis is induced by generated reactive oxygen species (ROS) from photosensitizers under specific light excitation [8,9].

Traditional photodynamic therapy is limited in clinical application due to the selection of ultraviolet or visible light as the excitation light source, which has poor tissue penetration depth [10,11]. The near-infrared region (700-1000 nm) has the advantages of deeper tissue penetration depth, higher imaging signal-to-noise ratio and resolution. It has become the best excitation light region for phototherapy and has been widely studied as the " optical window of biological tissue" [12-14]. Compared with organic photosensitizers (such as Ce6 and ZnPc), inorganic semiconductors (such as TiO_2, SnO_2, MnO_2, etc. [15-17]) have good biocompatibility, longer stability *in vivo* and no obvious toxicity. However, most of the semiconductors can only be absorbed under ultraviolet or visible light [18,19]. As a kind of semiconductor, $W_{18}O_{49}$ has strong light absorption in the near-infrared region due to its oxygen defect and LSPR effect [20-22]. KALLURU et al. [23] prepared $W_{18}O_{49}$ nanowires modified by PEG, which could sensitize the formation of singlet oxygen and completely destroy the solid tumor of mice when irradiated with 980 nm laser. However, due to the strong absorption of 980 nm near-infrared light by water, the thermal effect will damage the normal human tissue. In contrast, biological tissues have a low absorption intensity of NIR light at 808 nm, which can effectively overcome the shortcomings of overheating effect and poor penetration depth caused by 980 nm laser excitation source [24].

In this work, $W_{18}O_{49}$ were synthesized via a facile solvothermal route, using tungsten chloride as raw material and n-propanol as solvent. Under the irradiation of 808 nm laser, the photodynamic performance of $W_{18}O_{49}$ was investigated by varying concentrations and illumination time, and *in vitro* cell experiments of $W_{18}O_{49}$ were further explored.

2. Experimental

2.1. Materials

Tungsten chloride (WCl_6) was purchased from Shanghai Aladdin Reagent Co.Ltd.. N-propanol (C_3H_7OH) was obtained from Tianjin Fuyu Fine Chemical Co.Ltd.. 1, 3-Diphenylisobenzofuran (DPBF) was supplied by Shanghai MackLin Biochemical Co.Ltd.. Methyl thiazolyl tetrazolium (MTT) was provided by American Sigma Company. Phosphate buffered saline (PBS) was obtained from Beijing Boaotuoda Technology Co.Ltd.. Culture Medium was obtained from American Hyclone corporation. Fetal bovine serum was obtained from Thermo Fisher Company. All chemicals were analytical reagents and could be used directly without further purification. The experimental water was deionized water.

2.2. Synthesis of $W_{18}O_{49}$ nanoparticles

WCl_6 (0.3g) was dissolved in n-propanol (60 mL) to make a transparent yellow solution under magnetically stirring for about 30 min. The resulting solution was transferred into a 100 mL Teflon-lined stainless steel autoclave and maintained at 200 ^oC for 24 h. Finally, the product was washed with deionized water and ethanol each for three times to obtain $W_{18}O_{49}$ solution.

2.3. Assessment of $W_{18}O_{49}$ photodynamic performance

30 μL of DPBF ethanol solution (1 mg/mL) was mixed with 3 mL $W_{18}O_{49}$ solution (1 mg/mL). The resulting solution was irradiated by 808 nm near-infrared laser in the dark and stirred simultaneously. The irradiated samples were centrifuged at 8000 rpm for 10 min. A pipette was used to collect the supernatant after centrifugation, and the singlet oxygen production results of tungsten oxide were tested in different irradiation time.

2.4. Biocompatibility test of $W_{18}O_{49}$

The biocompatibility of $W_{18}O_{49}$ nanomaterial was determined by MTT array. First, L929 normal cells were seeded in a 96-well plate. $W_{18}O_{49}$ culture medium with different concentrations (0 mg/mL, 0.05 mg/mL, 0.1 mg/mL, 0.2 mg/mL, 0.5 mg/mL and 1 mg/mL) was used to culture cells in a 5% CO_2 humidity incubator at (37±1) □ for 24 h. After that, 20 μL of MTT stock solution was added into the pore plates which had different concentration gradients of samples. The pore plates were covered with aluminum foil to avoid direct light exposure, and cultured at 37 □ for 4 h. The changes of light and sample concentrations were experimental variables. The light condition was that samples were irradiated with 808 nm laser for 5 minutes. Finally, 150 μL of dimethyl sulfoxide (DMSO) was added to each well. The absorbance at 490 nm was examined by a microplate reader.

2.5. Characterization

The phase of the products was identified by X-ray diffraction (XRD, PANalytical X'Pert PRO MPD, Holland) with Cu-Kα radiation. The morphologies of nanomaterials were observed by transmission electron microscopy (TEM, JEM-2010, Japan) and scanning electron microscope (SEM, FEI Sirion 200, FEI). The fourier transform infrared (FT-IR, CZ304, Japan) was used to detect different functional groups. The products were excited by 808 nm laser provided by NINGBO LASEVER INC. The photodynamic performance of the samples was tested by UV-Vis spectrometer. The biocompatibility of samples was analyzed by GF-M3000 microplate reader., BC-J80S CO_2 Incubator and Vertical pressure steam sterilizer.

3. Result and discussion

Fig. 1 showed the XRD pattern of $W_{18}O_{49}$. Obviously, it could be seen that the samples had two distinct diffraction peaks, which were corresponded to the (010) crystal plane of $W_{18}O_{49}$ at 23.45° and the (020) crystal plane at 47.96°. $W_{18}O_{49}$ might grow along (010) crystal plane, since the diffraction peak intensity was the highest at 2θ=23.45°. The samples were basically consistent with the diffraction peaks of the PDF card (JCPDS 05-0392). Therefore, it could be concluded that the product was pure monoclinic $W_{18}O_{49}$ with high crystallinity.

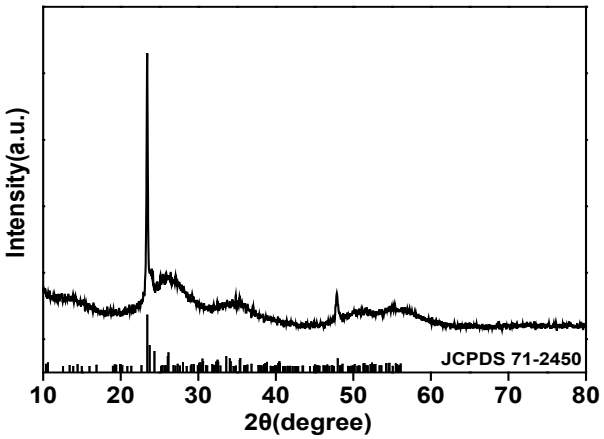

Fig. 1. XRD pattern of $W_{18}O_{49}$ sample.

In order to study the microstructure of $W_{18}O_{49}$ nanoparticles, the synthesized samples were characterized by SEM and TEM. Fig 2(a) was the SEM image of the $W_{18}O_{49}$ sample, and (b) was the TEM image of the sample. The results showed that the morphology of $W_{18}O_{49}$ was fusiform with no obvious agglomeration and uniform dispersion, about 500 nm in length and 100 nm in width. TEM image of $W_{18}O_{49}$, as an inset in Fig. 2(b), presented a distinct lattice fringe of about 0.38 nm, well in consistence with the (010) plane of $W_{18}O_{49}$. It was proved that $W_{18}O_{49}$ grew along the direction of (010) crystal plane.

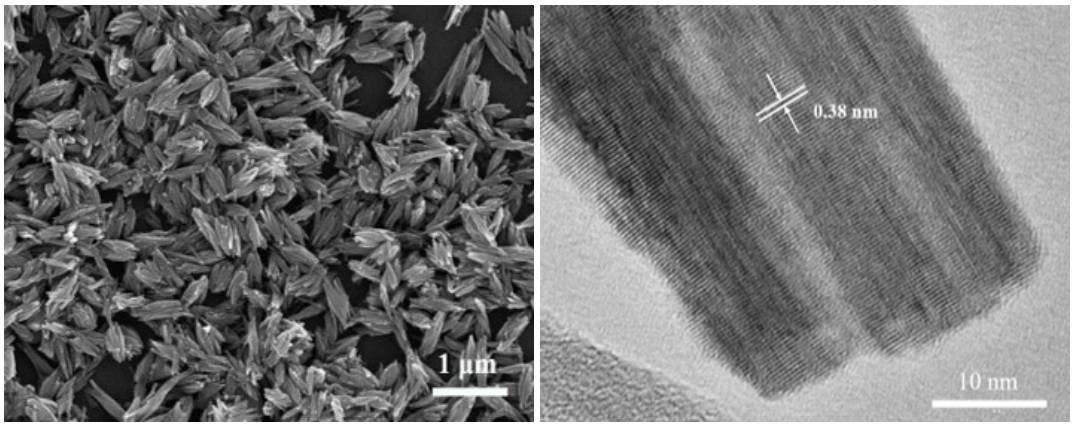

(a) *(b)*

Fig. 2. SEM and TEM images of $W_{18}O_{49}$; SEM image of $W_{18}O_{49}$ (b) TEM image of $W_{18}O_{49}$.

FT-IR spectroscopy was carried out to analyze chemical bond for $W_{18}O_{49}$. The infrared spectrum of $W_{18}O_{49}$ was showed in Fig. 3. According to the spectrum, the W-O and W-O-W characteristic absorption peaks of $W_{18}O_{49}$ were mainly observed in the region at 600-1000 cm^{-1}. The presence of the characteristic absorption peak at 660 cm^{-1} indicated the stretching vibration of W-O and the characteristic peaks at 737 cm^{-1} and 826 cm^{-1} were W-O-W bridging stretching mode, which had been reported in literature [25], confirming the successful synthesis of $W_{18}O_{49}$ nanoparticles.

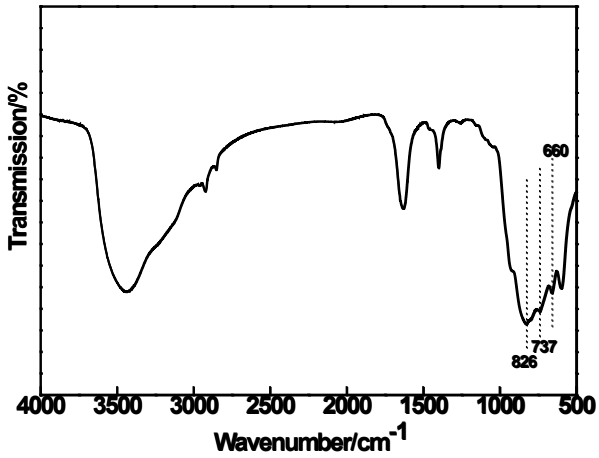

Fig. 3. FT-IR spectrum of $W_{18}O_{49}$.

To further explore the application potential of material in photodynamic cancer therapy, $W_{18}O_{49}$ samples were tested by the UV-Vis-NIR diffuse reflection spectrum. As described in Fig. 4, a strong light absorption in the ultraviolet region of 200-380 nm was found in $W_{18}O_{49}$ and a high absorption in the near infrared region of 780-1200 nm which had a deep tissue penetration was also found in $W_{18}O_{49}$. The light absorption capacity of $W_{18}O_{49}$ nanoparticles was increased by increasing the wavelength. $W_{18}O_{49}$ application was limited due to the poor penetration depth of tissue by ultraviolet or visible light while near-infrared light was the best light-excitation region for tumor phototherapy, indicating the potential of $W_{18}O_{49}$ to become a phototherapy agent with its excellent near-infrared absorption performance.

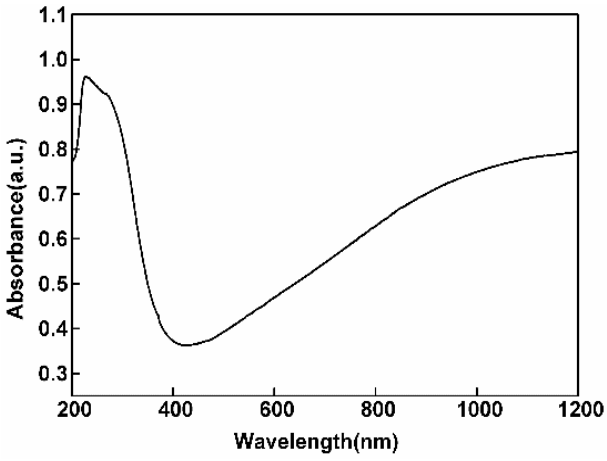

Fig. 4. UV-Vis-NIR spectrum of $W_{18}O_{49}$.

The efficient generation of singlet oxygen was an important factor for photodynamic therapy to kill tumor cells. DPBF was a singlet oxygen capture agent, which had a characteristic absorption peak at 419 nm. The absorption peak of DPBF was decreased due to the generation of

singlet oxygen. Therefore, the photodynamic performance of the samples was investigated by detecting the change in the absorption peak of DPBF at 419 nm. As shown in Fig 5, the singlet oxygen generation capacity of $W_{18}O_{49}$ dispersions with different concentrations was tested under NIR-808 nm light irradiation for 15 min. With the increase of the sample concentration, the absorbance of DPBF was gradually decreased, which verified that $W_{18}O_{49}$ photosensitizer was stimulated by the NIR light to generate singlet oxygen. It could be seen from the figure that with the increase of sample concentration, the decomposition rate of DPBF became slower and the generation of singlet oxygen was decreased. When the concentration was reached 1 mg/mL, the absorption peak of DPBF was tended to be horizontal, indicating that DPBF was almost completely decomposed. Therefore, the production of singlet oxygen was increased by increasing the concentration of sample and the photodynamic effect was better.

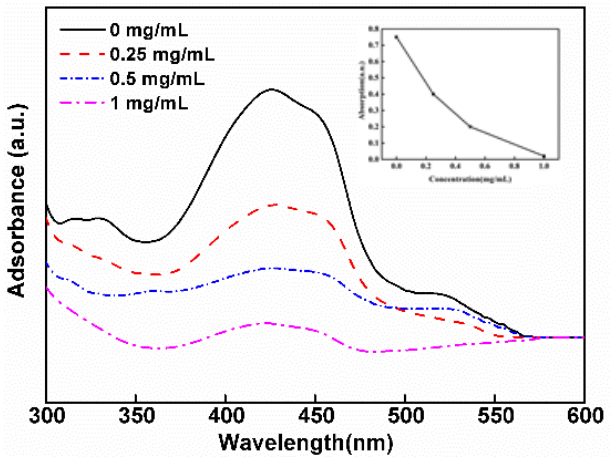

Fig. 5. Absorption spectra of DPBF with different concentrations of $W_{18}O_{49}$ (inset is the plot of change in absorption).

When the sample concentration was 1 mg/mL, the photodynamic effect was the best. Then, the influence of illumination time on the photodynamic performance was explored at this concentration, as shown in Fig 6. The stock solution in the figure represented the mixed solution of water and DPBF in dark, and its UV absorption peak intensity at 419 nm was basically the same as that of $W_{18}O_{49}$ solution without light. The results showed that the singlet oxygen could not be produced by chemical reaction in the system under no light condition. Under NIR-808 nm laser irradiation, the UV absorption of the sample solution was measured every 5 min. With the increase of illumination time, the absorbance of DPBF mixed solution was decreased significantly at 419 nm. As can be seen from Fig 5, with the increase of time, the absorbance decline rate was gradually decreased, that was, the decomposition rate of DPBF was slowed down and the rate of singlet oxygen generation was decreased. After 15 min of light irradiation, the absorption peak of DPBF at 419 nm was decreased significantly, and the absorbance was decreased. It showed more singlet oxygen was produced with longer illumination time and the photodynamic effect was significant.

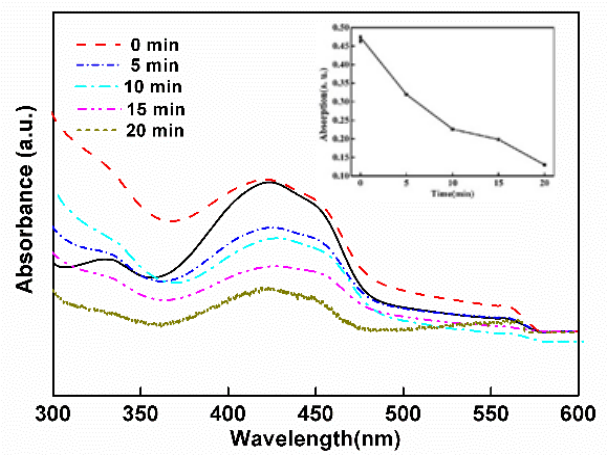

Fig. 6. Absorption spectra of DPBF with different irradiation time (inset is the plot of change in absorption).

A good photosensitizer not only had the ability to produce singlet oxygen, but also needed good photodynamic stability. In order to further evaluate the photodynamic stability of $W_{18}O_{49}$ nanoparticles, changes in absorption intensity of DPBF solution under near-infrared laser irradiation were shown in Fig. 7. The light absorption intensity of DPBF was changed very little under four cycles of laser irradiation with 808 nm, which indicated that $W_{18}O_{49}$ nanoparticles had good singlet oxygen generation ability and photodynamic stability.

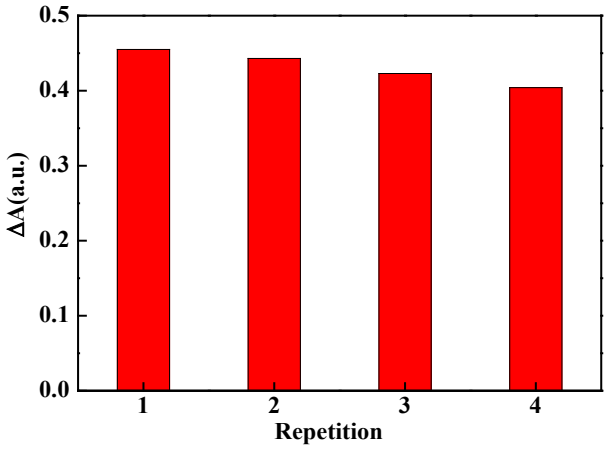

Fig. 7. The Photodynamic stability of $W_{18}O_{49}$ samples under 808 nm near infrared light irradiation.

The methyl thiazolyl tetrazolium (MTT) assay was used to determine the biocompatibility of $W_{18}O_{49}$ nanomaterials. The *in vivo* experiment result was displayed in Fig. 8, which showed the MTT figure of $W_{18}O_{49}$ and L929 normal cells co-cultured for 24 h at different concentrations (0.05, 0.1, 0.2, 0.5 and 1 mg/mL). The control experiment was conducted with no light and the irradiation of 808 nm near-infrared light. The cell viability was higher than 100% in the dark. The cell viability was not affected by the increase of sample concentration and the cell proliferation was normal. Under the irradiation of 808 nm near-infrared light, the cell viability was decreased

slightly with the increase of sample concentration. When the sample concentration was arrived at 1 mg/mL, the cell viability was still above 90%. There was almost no damage to normal tissue cells when treated with the samples and light conditions.

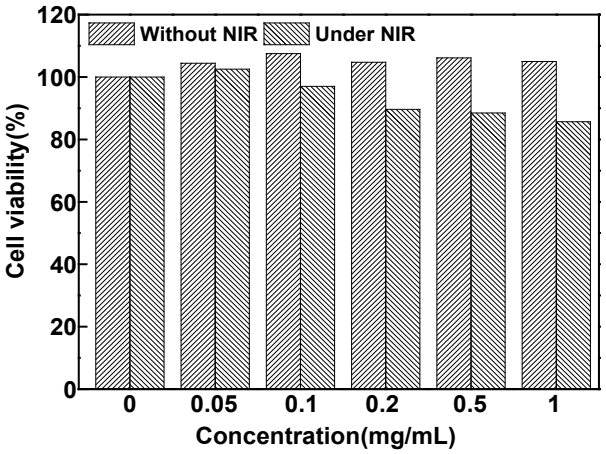

Fig. 8. The viabilities of L929 cells co-cultured with $W_{18}O_{49}$ for 24 h.

$W_{18}O_{49}$ and MCF-7 tumor cells were co-cultured for 24 h when the irradiation of near-infrared light and sample concentration were used as comparison conditions. As shown in Fig. 9, there were 100% viabilities in MCF-7 tumor cells which exposed with 808 nm laser irradiation only or incubated with $W_{18}O_{49}$ in dark, indicating that MCF-7 tumor cells were not inhibited by $W_{18}O_{49}$ only or light and the cells could be proliferated normally. However, with the increase of $W_{18}O_{49}$ concentration under the irradiation of 808 nm laser light, the viabilities of tumor cells were decreased gradually. When the concentration of $W_{18}O_{49}$ was increased to 1 mg/mL, the cell viability was 35% after 5 min irradiation, which effectively inhibited the growth of tumor cells. In conclusion, the $W_{18}O_{49}$ nanoprobe showed good biocompatibility for normal tissue cells and an evident inhibition effect on tumor cells under 808 nm near-infrared light, which had the application potential in photodynamic cancer therapy.

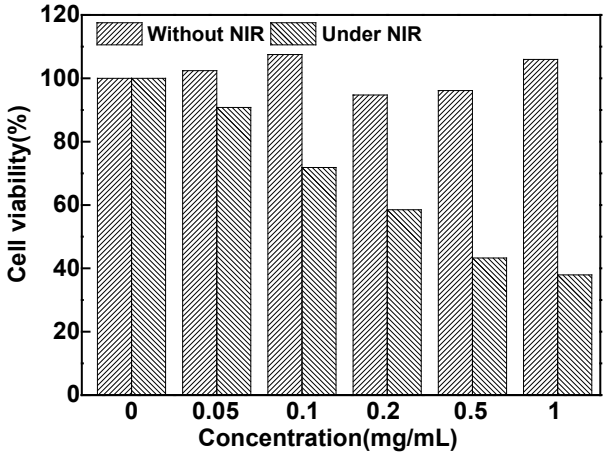

Fig. 9. The viabilities of MCF-7 tumor cells co-cultured with $W_{18}O_{49}$ for 24 h.

4. Conclusions

In summary, non-stoichiometric nano-tungsten oxide with spindle morphology was prepared by the solvothermal method, which possessed high crystallinity, good dispersibility, uniform sizes and evident absorption of NIR light. The photodynamic performance results showed that under the irradiation of NIR-808 nm, with the increase of irradiation time and sample concentration, the production of singlet oxygen in the system was increased, and it had the photodynamic effect which could generate reactive oxygen species effectively. MTT *in vitro* experiments indicated that the $W_{18}O_{49}$ nanoprobe had good biocompatibility with normal tissue cells and could effectively inhibit tumor cells under the irradiation of 808 nm laser light, which had a wide application prospect in photodynamic cancer therapy.

Acknowledgements

This work was financially supported by the Natural Science Foundation of China Youth Program (51603057), the Natural Science Joint Foundation of Shandong Province (ZR2021LSW014), Heilongjiang University Students Innovation and Entrepreneurship Experimental Training Project (202010214147).

References

[1] Y. E. Xue, J. Y. Che, X. M. Ji, Y. N. Li, J. B. Xie, X. Y. Chen, Chemical Society Review, 51(05), 1766 (2022); https://doi.org/10.1039/D1CS00786F

[2] M. Zou, Y. Q. Chen, Journal of Materials Engineering 48(09), 59 (2020).

[3] W. J. Yu, P. Geng, M. Wen, Z. G. Chen, Journal of Materials Engineering 48(12), 68 (2020).

[4] E. Darrigues, Z. A. Nima, R. J. Griffin, J. M. Anderson, A. S. Biris, A. Rodriguez, Nanoscale Horizon 5(03), 400 (2020); https://doi.org/10.1039/C9NH00628A

[5] C. Xu, K. Y. Pu, Chemical Society Reviews 50(02), 1111 (2021); https://doi.org/10.1039/D0CS00664E

[6] L. Huang, S. J. Zhao, J. S. Wu, L. Yu, N. Singh, K. Yang, M. H. Lan, P. F. Wang, J. S. Kim, Coordin Chem Rev 438, 213888 (2021); https://doi.org/10.1016/j.ccr.2021.213888

[7] H. X. Lin, Z. X. Lin, K. H. Zheng, C. L. Wang, L. S. Lin, J. X. Chen, J. B. Song, Advanced Optical Materials 9(09), 2002177 (2021); https://doi.org/10.1002/adom.202002177

[8] S. K. Liu, W. T. Li, S. M. Dong, S. L. Gai, Y. S. Dong, D. Yang, Y. L. Dai, F. He, P. P. Yang, ACS applied materials & interfaces 11(51), 47659 (2019); https://doi.org/10.1021/acsami.9b11973

[9] S. Shao, B. B. Ding, Z. L. Zhu, P. A. Ma, J. Lin, Chinese Journal of Analytical Chemistry 47(06), 823 (2019).

[10] W. P. Fan, P. Huang, X. Y. Chen, Chemical Society Reviews 45(23), 6488 (2016); https://doi.org/10.1039/C6CS00616G

[11] E. Kohl, C. Popp, F. Zeman, P. Unger, M. Koller, M. Landthaler, S. Karrer, R. M. Szeimies, British Journal Dermatology 176(02), 352 (2017); https://doi.org/10.1111/bjd.14970

[12] M. Broekgaarden, R. Weijer, W. Van, R. C. Cox, M. R. Egmond, R. Hoebe, T. M. van Gulik, M. Heger, Journal of Biomedical Nanotechnology 13(02), 204 (2017); https://doi.org/10.1166/jbn.2017.2327

[13] T. T. Xu, J. H. Li, F. R. Cheng, Y. X. Zhang, J. Cao, W. X. Gao, B. He, Chinese Chemical Letters 28(09), 1885 (2017); https://doi.org/10.1016/j.cclet.2017.07.029

[14] M. Y. Chang, Z. Y. Hou, M. Wang, C. Z. Yang, R. F. Wang, F. Li, D. L. Liu, T. L. Peng, C. X Li, J. Lin, Angewandte Chemie International Edition 60(23), 2 (2021); https://doi.org/10.1002/anie.202101924

[15] N. Yu, C. Peng, Z. J. Wang, Z. X. Liu, B. Zhu, Z. G. Yi, M. F. Zhu, X. G. Liu, Z. G. Chen, Nanoscale 10(05), 2542 (2018); https://doi.org/10.1039/C7NR08811F

[16] L. S. Lin, J. B. Song, L. Song, K. M. Ke, Y. J. Liu, Z. J. Zhou, Z. Y. Shen, J. Li, Z. Yang, W. Tang, G. Niu, H. H. Yang, X. Y. Chen, Angewandte Chemie-International Edition 57(18), 4902 (2018); https://doi.org/10.1002/anie.201712027

[17] Y. Y. Jiang, P. K. Upputuri, C. Xie, Z. L. Zeng, A. Sharma, X. Zhen, J. C. Li, J. G. Huang, M. Pramanik, K. Y. Pu, Advanced Materials 31(11), 1808166 (2019); https://doi.org/10.1002/adma.201808166

[18] M. Feng, R. C. Lv, L. Y. Xiao, B. Hu, S. P. Zhu, F. He, P. P. Yang, J. Tian, Inorganic Chemistry 57(23), 14594 (2018); https://doi.org/10.1021/acs.inorgchem.8b02257

[19] M. Y. Chang, Z. Y. Hou, M. Wang, M. F. Wang, P. P. Dang, J. H. Liu, M. M. Shu, B. B. Ding, A. A. Al Kheraif, C. X. Li, J. Lin, Small 16(14), 1907146 (2020); https://doi.org/10.1002/smll.201907146

[20] H. Y. Fu, X. J. Li, W. Sun, D. Y. Liu, X. F. Gao, L. M. Dong, H. T. Fu, Journal of Nano Research 67, 81 (2021); https://doi.org/10.4028/www.scientific.net/JNanoR.67.81

[21] X. F. Gao, X. J. Li, D. Y. Liu, Acta Materiae Compositae Sinica 38(09), 2965 (2021).

[22] W. C. Huang, J. X. Wang, L. Bian, C. Y. Zhao, D. Q. Liu, C. S. Guo, B. Yang, W. W. Cao, Physical Chemistry Chemical Physical 20(25), 17268 (2018); https://doi.org/10.1039/C8CP02044B

[23] P. Kalluru, R. Vankayala, C. S. Chiang, K. C. Hwang, Angewandte Chemie International Edition 52(47), 12332 (2013); https://doi.org/10.1002/anie.201307358

[24] Y. F. Wang, G. Y. Liu, L. D. Sun, J. W. Xiao, J. C. Zhou, C. H. Yan, ACS Nano 7(08), 7200 (2013); https://doi.org/10.1021/nn402601d

[25] K. N. Song, F. Xiao, L. J. Zhang, F. Yue, X. Y. Liang, J. D. Wang, X. T. Su, Journal of Molecular Catalysis A: Chemical 418, 95 (2016); https://doi.org/10.1016/j.molcata.2016.03.029